forests

MDPI

Article

The Effects of Dynamic Root Distribution on Land–Atmosphere Carbon and Water Fluxes in the Community Earth System Model (CESM1.2.0)

Yuanyuan Wang [1,2], Binghao Jia [2,*] and Zhenghui Xie [2]

1 Beijing Meteorological Observatory, Beijing 100089, China; wangyuanyuan@mail.iap.ac.cn
2 State Key Laboratory of Numerical Modeling for Atmospheric Sciences and Geophysical Fluid Dynamics (LASG), Institute of Atmospheric Physics, Chinese Academy of Sciences, Beijing 100029, China; zxie@lasg.iap.ac.cn
* Correspondence: bhjia@mail.iap.ac.cn; Tel.: +86-10-82995452

Received: 30 January 2018; Accepted: 23 March 2018; Published: 29 March 2018

Abstract: Roots are responsible for the uptake of water and nutrients by plants, and they have the plasticity to respond dynamically to different environmental conditions. However, currently, most climate models only prescribe rooting profiles as a function of the vegetation type of the land component, with no consideration of the surroundings. In this study, a dynamic rooting scheme describing root growth as a compromise between water and nitrogen availability in the subsurface was incorporated into the Community Earth System Model 1.2.0 (CESM1.2.0). The dynamic rooting scheme was incorporated to investigate the effects of land–atmosphere carbon and water fluxes, and their subsequent influences on climate. The modeling results of global land–atmosphere coupling simulations from 1982 to 2005 show that the dynamic rooting scheme can improve gross primary production (GPP) and evapotranspiration (ET) in most tropical regions, and in some high-latitude regions with lower mean biases (MBEs) and root mean square errors (RMSEs). Obvious differences in 2-m air temperature were found in low-latitude areas, with decreases of up to 2 °C. Under the influence of local land-surface feedback and large-scale moisture advection, total precipitation in the northeastern area of the Amazon and the west coast of Africa increased by 200 mm year^{-1}, and that of South America, central Africa, and Indonesia increased by 50 to 100 mm year^{-1}. Overall, the model incorporating the dynamic rooting scheme may reveal cooling and humidifying effects, especially for tropical regions.

Keywords: dynamic root distribution; CLM4.5; CESM1.2.0; global climate

1. Introduction

Plants are the main component of the terrestrial biosphere, and can affect climate through matter and energy exchange between the land surface and the atmosphere. Photosynthesis and plant respiration can influence carbon exchange between the land surface and the atmosphere, and therefore can affect the global carbon balance by adjusting atmospheric carbon dioxide (CO_2) concentration. Furthermore, interception and transpiration of water by plants can change the distribution of water by altering evaporation, runoff, soil water, and groundwater, thereby regulating water and heat exchange between the land surface and the atmosphere, ultimately changing the climate [1–4]. Roots are one of the most important components of plants; they couple the aboveground vegetation and the soil media, and connect the soil environment to the atmosphere through water and energy flux exchanges between the vegetation canopy and the atmosphere. Moreover, roots are also responsible for nutrient uptake, which may control carbon (C) synthesis [5].

It is important to understand the role that roots play in global carbon and hydrological cycles, and their subsequent influence on climate. Unfortunately, roots are arguably the least understood portion of both the ecosystem and land-surface processes. As a result, they are represented idealistically in many process-based land-surface models (LSMs), and remain the most simplistic component of contemporary Earth system models (ESMs). The vertical distribution of roots, which is one of their most important properties, is an essential component of many eco-hydrological models [6] and LSMs [7–9]; it mainly controls the extent of root water uptake among soil layers, and therefore soil water stress. Soil water stress further influences transpiration, C assimilation, and subsequently other C and water fluxes [10–12]. Hence, a realistic representation of root distribution is very important for hydrological, ecological, and climate modeling [13–18]. Due to the difficulty of measuring entire root distributions throughout the soil profile [18,19], the root distribution in most LSMs is simplified and treated as a static component [11,19]. The parameters in static root distribution schemes depend only on plant type, with root distributions spatially and temporally invariant. It has been demonstrated that plants tend to allocate C to enhance acquisition of a limited resource [20], and therefore tend to grow more roots in zones where soil moisture is more freely available [21–23], and where more nutrients can be acquired [24]. These observations imply that root systems have the plasticity to respond dynamically to environmental conditions such as water and nutrient availability [25–27], indicating that static schemes are insufficient to describe actual root distributions and need to be improved. Wang et al. [28] incorporated a dynamic root scheme into the Community Land Model version 4.5 (CLM4.5) that describes root growth as a compromise between water and nitrogen availability, and investigated the effects of dynamic root distribution on eco-hydrological modeling in the Amazon. Their results showed that vegetation responses to seasonal drought were better captured by the new dynamic root distribution scheme.

Despite this, feedback loops among roots, soil, and vegetation are expected to influence ecosystem responses to climate change. Therefore, there is an urgent need for scientists to improve prognostic approaches to understand how roots govern changes in resource availability, and how root responses influence climate. In this study, the dynamic root distribution scheme mentioned above [28] was incorporated into the Community Earth System Model version 1.2.0 (CESM1.2.0), to further investigate the effects of dynamic root distribution on global climate, and the analysis focused on gross primary production (GPP), evapotranspiration (ET), 2-m air temperature (TA), and land precipitation (PR).

2. Methods

2.1. Model Development

2.1.1. The Community Earth System Model

The CESM1.2.0 [29] was developed from the Community Climate System Model, version 4 (CCSM4). It consists of seven geophysical models: atmosphere, land, ocean, land-ice, runoff, sea-ice, and ocean-wave, linked by a coupler that passes information among them. The atmospheric component is the Community Atmosphere Model, version 4 (CAM4) [30], which uses the Lin–Rood finite-volume dynamic core with an atmospheric grid spacing of $0.9^\circ \times 1.25^\circ$ horizontally, and 26 levels in the vertical direction arranged in a hybrid pressure sigma coordinate system [31]. The land component, CLM4.5, which is a state-of-the-art LSM, is the latest version of the CLM family of models. The spatial heterogeneity of the land surface is represented in CLM as a nested sub-grid hierarchy, and vegetation is classified into 16 plant functional types (PFTs) according to different photosynthesis parameters and optical properties. This model can simulate the exchange of radiation, momentum, heat, and water-vapor flux between the land and the atmosphere, as well as hydrologic processes (including precipitation interception, soil water infiltration, and so on). CLM4.5 also has a biogeochemistry module called the carbon–nitrogen cycle (C–N) model, which is fully prognostic with respect to all C and N state variables in vegetation, litter, and soil organic matter, to provide an explicit description of

photosynthesis, respiration, and plant phenology [32]. A detailed description of its biogeophysical and biogeochemical parameterizations and numerical implementation can be found in Oleson et al. [33].

The root distribution function that determines the fraction of roots (r_i) in each soil layer in CLM4.5 can be written as follows [34]:

$$r_i = \left\{ \begin{array}{ll} 0.5\left[\begin{array}{l} \exp(-r_a z_{h,i-1}) + \exp(-r_b z_{h,i-1}) - \\ \exp(-r_a z_{h,i}) - \exp(-r_b z_{h,i}) \end{array} \right] & \text{for } 1 \le i < 10 \\ 0.5[\exp(-r_a z_{h,i-1}) + \exp(-r_b z_{h,i-1})] & \text{for } i = 10 \end{array} \right\} \quad (1)$$

where $z_{h,i}$ (m) is the depth from the soil surface to the interface between layer i and $i + 1$; r_a and r_b are two PFT-dependent root parameters.

2.1.2. Dynamic Rooting Scheme and Its Implementation

At present, although the root C pool does vary temporally, due to the static rooting scheme, there is no net change in the root fraction within each soil layer. To represent actual dynamic root growth, the dynamic rooting scheme developed by Wang et al. [28] was incorporated into CESM1.2.0 by integrating it into the land component (i.e., the CLM4.5 land-surface model). This scheme enables the total new root C gain at each time step to be dynamically allocated to each soil layer according to the surrounding environment, achieving a compromise between soil water and soil mineral N, as expressed by Equation (2):

$$\Delta C_{fr,i} = \Delta C_{fr}[(1 - \beta_t) \frac{w_i \Delta z_i}{\sum_{j=1}^{10} w_j \Delta z_j} + \beta_t \frac{n_i \Delta z_i}{\sum_{j=1}^{10} n_j \Delta z_j}] \quad (2)$$

where ΔC_{fr} (units: g C m^{-2} s^{-1}) is the newly assimilated C allocated to roots, Δz_i (units: m) is the soil layer thickness, n_i (units: g N m^{-3}) is soil mineral N content, and w_i is the plant wilting factor of layer i. β_t is the soil water stress due to water deficiency, which depends on w_i and the root fraction (r_i) and can be expressed as:

$$\beta_t = \sum_{i=1}^{10} w_i r_i \quad (3)$$

$$w_i = \frac{\psi_c - \psi_i}{\psi_c - \psi_o} \frac{\theta_{sat,i} - \theta_{ice,i}}{\theta_{sat,i}} \quad (4)$$

where Ψ_i is the soil water matric potential (units: mm), and Ψ_c and Ψ_o are the soil water potential (units: mm) when stomata are fully closed or fully open, respectively. $\theta_{sat,i}$ and $\theta_{ice,i}$ are the saturated volumetric water and ice contents, respectively (units: m^3 m^{-3}). The function β_t ranges from 0 to 1, with larger values indicating higher water availability. The root distribution after the new dynamic allocation is then updated based on the amount of roots C ($C_{fr,i}$; units: g C m^{-2}) in layer i and the total amount of roots C ($\sum_{i=1}^{10} C_{fr,i}$; units: g C m^{-2}):

$$r_i = \frac{C_{fr,i}}{\sum_{i=1}^{10} C_{fr,i}} \quad (5)$$

As the vertically resolved soil mineral N is not predicted in CLM4.5, the total N (TN) data from the Global Soil Dataset for Earth System Modeling [35] that had vertical layers consistent with CLM4.5 were used to represent soil mineral N content [28]. Although this data was time invariant, more effort should be made to resolve the original CLM4.5 TN in order to produce vertically layered data in the future. The dynamic rooting scheme influences climate modeling in CESM1.2.0 in multiple ways.

The varying root distribution has a direct impact on β_t, which affects photosynthesis and stomatal conductance. Moreover, the varying root fraction influences the effective root fraction, which affects the amount of water extracted from each layer. The aforementioned factors will ultimately influence land–atmosphere exchange processes, such as transpiration, and through these will affect latent heat, gross primary production, and the global climate. Figure 1 shows in detail the impacts of the dynamic rooting scheme on land–atmosphere interactions.

It should be noted that in CLM4.5, the carbon allocation for new growth is only based on the allometric parameters, depending on PFTs. However, when vegetation was restricted by light, more carbon would be allocated to the stems; when restricted by water or nutrients, more carbon would be distributed to the roots. In this study, we only considered the change of root carbon allocation between different soil layers with environmental factors, and did not consider the dynamic changes of carbon allocation between leaves, stems, and roots.

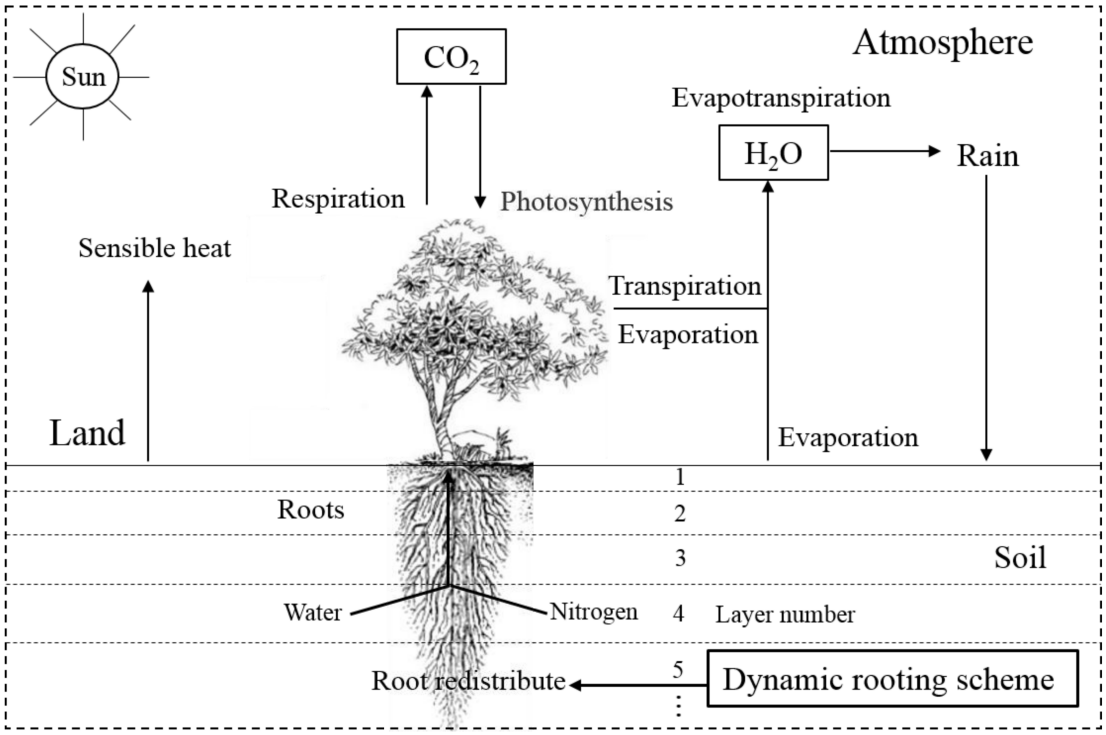

Figure 1. Schematic diagram of the impacts of the dynamic rooting scheme on land–atmosphere interactions.

2.2. Experimental Design

In order to investigate the effects of root dynamics on global climate, two sets of numerical experiments were conducted using the original CESM1.2.0 (referred as CTL) and CESM1.2.0_DR coupled with the dynamic rooting scheme (referred as NEW). In these experiments, only the atmospheric (CAM4) and land (CLM4.5) components were integrated, whereas ocean surface conditions were prescribed using monthly observations of sea-surface temperatures (SSTs) and sea-ice concentration from the HadISST dataset [36]. To establish the C and N pools and fluxes, the 1000-year initialization results were used as initial conditions. The greenhouse gas forcing data are from the 2000 observations, and the land-use data are derived from the Moderate Resolution Imaging Spectroradiometer satellite data. The monthly results at $0.9^\circ \times 1.25^\circ$ resolution, from 1982 to 2005, were analyzed, focusing on gross primary production (GPP), evapotranspiration (ET), 2-m air temperature (TA), and land precipitation (PR). Here, the Model Tree Ensembles (MTE) datasets were used as a reference for benchmarking these comparisons: The global GPP and ET (monthly, $0.5^\circ \times 0.5^\circ$) were up-scaled from FLUXNET observations using a machine-learning technique for 1982–2010 [37,38].

The precipitation data (from 1901 to 2014, monthly, 1° × 1°) from the Global Precipitation Climatology Centre (GPCC) (https://www.esrl.noaa.gov/psd/data/gridded/data.gpcc.html#detail), and the air temperature reanalysis data (from 1948 to 2014, monthly, 0.5° × 0.5°) from the National Centers for Environmental Prediction (NCEP), were also used as benchmarks.

2.3. Mathematical Indices of Model Performance

Three indices were used to evaluate the agreement between model simulations and observations: the correlation coefficient (R), the mean bias error (MBE), and the root mean square error (RMSE). The three indices are defined as follows:

$$R = \frac{\sum_{i=1}^{N}(x_i - \overline{x})(\mathrm{obs}_i - \overline{\mathrm{obs}})}{\sqrt{\sum_{i=1}^{N}(x_i - \overline{x})^2}\sqrt{\sum_{i=1}^{N}(\mathrm{obs}_i - \overline{\mathrm{obs}})^2}} \quad (6)$$

$$\mathrm{MBE} = \frac{\sum_{i=1}^{N}(x_i - \mathrm{obs}_i)}{N} \quad (7)$$

$$\mathrm{RMSE} = \sqrt{\frac{\sum_{i=1}^{N}(x_i - \mathrm{obs}_i)^2}{N}} \quad (8)$$

where x is a model simulation either from CTL or NEW, obs is the corresponding observation, and $\overline{x}$ and $\overline{\mathrm{obs}}$ are the mean of x and obs respectively. RMSE provides an estimate of the absolute bias in the model simulation; the smaller the value of RMSE, the better is the agreement between simulation and observations.

3. Results and Discussion

3.1. Effects on Land Variables

Figure 2 shows the spatial distributions of the 24-year (1982–2005) mean soil moisture (SM, $m^3\ m^{-3}$) from model simulations (CTL and NEW), and the difference between them. Both the CTL and NEW runs show the same spatial pattern of global SM, with higher values in humid and semi-humid areas, and lower values in arid and semi-arid areas. When the dynamic root distribution was incorporated, SM in most regions decreased by up to 0.02 $m^3\ m^{-3}$, whereas SM in high-latitude regions increased, mainly because of changes in soil water stress (β_t), due to variations in the root fraction. Similarly to Figure 2, Figure 3 shows the spatial distributions of 24-year mean sensible heat (SH, W m^{-2}). SH for global land was found to be positive, which meant that heat was transferred from the land to the atmosphere on average, with larger values in the tropics and smaller values in the middle and high latitudes (Figure 3a,b), in accordance with surface temperature. In the NEW run, SH decreased in tropical regions by up to 20 W m^{-2}, and the regions with significant changes matched well with those with significant 2-m air temperature decreases (see Section 3.2). Figure 4 shows the spatial distributions of 24-year (1982–2005) mean evapotranspiration (ET, mm $year^{-1}$) from the CTL and NEW model simulations (denoted as CTL_ET and NEW_ET), MTE data (MTE_ET), and the differences between them. The spatial patterns of simulated ET were very similar (Figure 4a,b) and decreased with increasing latitude, consistently with MTE_ET (Figure 4c). This meant that the largest annual ET was found in tropical regions, followed by mid-latitude and high-latitude regions, except for bare soil. The spatial correlation coefficients between the simulated ET with MTE_ET were 0.88 for CTL and 0.90 for NEW (both significant at the 99% confidence level, $p < 0.01$), but CTL_ET was underestimated in low-latitude regions. The annual global ET values predicted by the two simulations were 372.1 mm $year^{-1}$ and 399.5 mm $year^{-1}$ respectively, which were much lower than the 496.5 mm $year^{-1}$

of MTE_ET, albeit with an obvious increase in NEW_ET. When the dynamic root distribution was considered, ET in most tropical regions increased, especially in South America and central Africa (Figure 4b), and the ET simulation improved. The overall effect was that dynamic root growth enhanced total evapotranspiration; this was due to increased transpiration and evaporation from vegetation in these areas for the NEW run (not shown), although soil evaporation was weakened to some extent. Five regions with significant differences in ET are framed with red lines in Figure 4d and denoted as R1, R2, R3, R4, and R5. The mean evaporation rates of MTE products for the five typical regions were 338.4 mm year^{-1}, 1268.2 mm year^{-1}, 1064.1 mm year^{-1}, 388.2 mm year^{-1}, and 888.7 mm year^{-1}. R2, which was located in South America, had the highest evapotranspiration rate, followed by R3 in South Africa. The ET rates of the CTL runs for the five regions were 299.9 mm year^{-1}, 1059.5 mm year^{-1}, 890.2 mm year^{-1}, 370.1 mm year^{-1}, and 994.8 mm year^{-1}. Compared with the MTE product, CTL_ET values for regions R1, R2, R3, and R4 were all underestimated, except for R5, where there was a slight overestimation. When dynamic root growth was taken into account, the ET underestimations for regions R1, R2, and R3 were improved, with their RMSEs reduced by 15.6 mm year^{-1}, 96.4 mm year^{-1}, and 56 mm year^{-1} (Table 1), but the ET in R4 was further underestimated, and the overestimation in R5 was not improved. In R5, the new rooting scheme let more water be absorbed by plants, causing water stress in the region to weaken, resulting in higher ET. Although, in south China, phosphorus may be the main limiter for carbon allocation (Wang et al., 2015), the model did not take this into account, which may have led to an unreasonable root profile, and an inaccurate ET estimation. In R4, the water stress was heavier when considering the dynamic rooting scheme, with less soil water absorbed for ET, so the ET simulation for this region by the NEW run was further underestimated. In R2 and R3, it was interesting that the R values were relatively lower (Jung et al., 2009). We found that both regions were characterized by a relatively sparse network of towers; however, the MTE algorithm strongly relied on observations, so this may be one reason why the MTE data did not match well with the mechanism-based model simulations. On the other hand, the plant types in the tropical regions were abundant, and the PFTs data used in this study may also deviate from the observations.

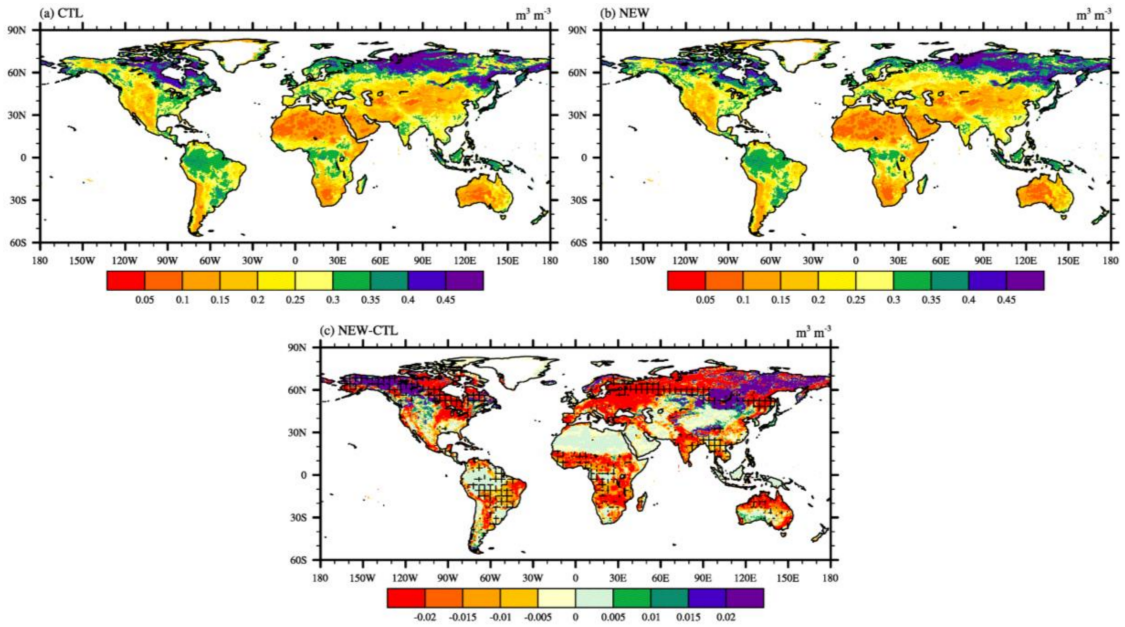

Figure 2. Annual soil moisture (SM, m^3 m^{-3}) over 1982–2005 for (**a**) the original CESM1.2.0 (CTL) run; (**b**) the CESM1.2.0_DR coupled with the dynamic rooting scheme (NEW) run; (**c**) the difference between NEW and CTL. (Grid shaded regions are significant at the 95% confidence level according to Student's *t*-test.).

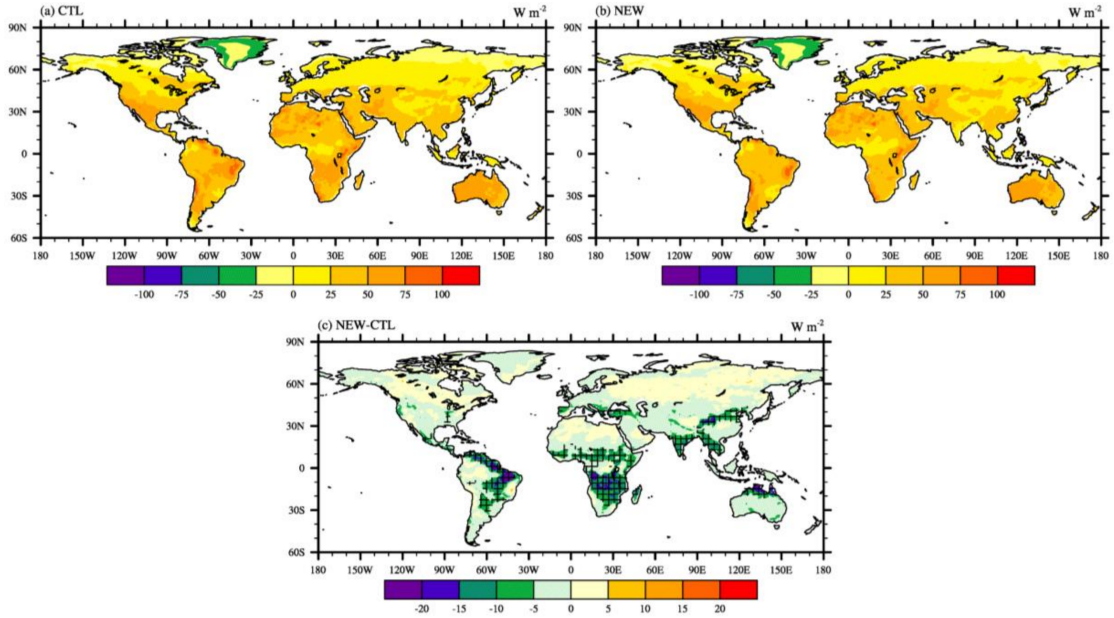

Figure 3. Annual sensible heat (SH, W m^{-2}) over 1982–2005 for (**a**) the CTL run; (**b**) the NEW run; (**c**) the difference between NEW and CTL. (Grid shaded regions are significant at the 95% confidence level according to Student's *t*-test.).

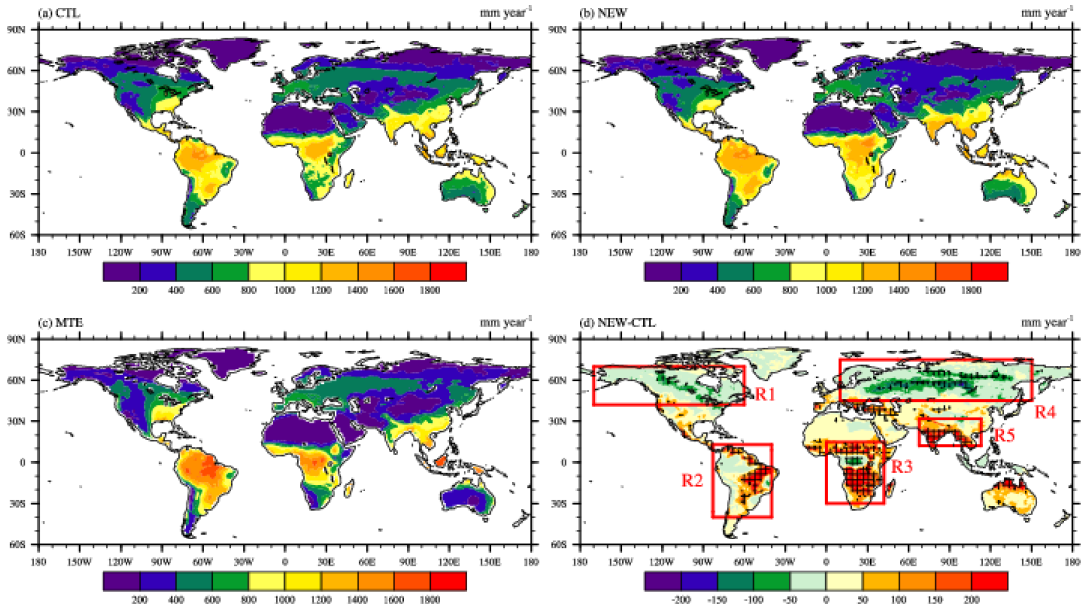

Figure 4. Annual evapotranspiration (ET, mm $year^{-1}$) over 1982–2005 for (**a**) the CTL run; (**b**) the NEW run; (**c**) Model Tree Ensembles (MTE); (**d**) the difference between NEW and CTL. (Grid shaded regions are significant at the 95% confidence level according to Student's *t*-test, and the red frames outline typical regions with significant differences, denoted as R1, R2, R3, R4, and R5.).

Table 1. Statistical characteristics of annual ET for five typical regions compared to MTE data. (Values with asterisks represent *R* with significance at the 95% confidence level ($p < 0.05$). Units for mean biases (MBE) and root mean square errors (RMSE) are in mm year^{-1}.)

	R1		R2		R3		R4		R5	
	CTL	NEW	CTL	NEW	CTL	NEW	CTL	NEW	CTL	NEW
R	0.86 *	0.88*	0.75	0.77	0.59	0.60	0.85 *	0.86 *	0.76	0.77
MBE	−37.61	−20.89	−208.6	−98.4	−60.1	−30.3	−18.1	−36.6	70.2	81.5
RMSE	51.3	35.7	226.5	130.1	151.3	95.3	41.3	91.5	112.1	191.3

Figure 5 shows the spatial patterns of mean GPP. Both the CTL and NEW simulations of GPP (denoted as CTL_GPP and NEW_GPP) and the benchmarking products (MTE_GPP) showed broadly similar patterns, with apparent latitude-related characteristics because ET decreased with increasing latitude. The spatial correlation coefficients between the simulated GPP and the MTE_GPP were 0.86 for CTL and 0.89 for NEW (both significant at the 99% confidence level, $p < 0.01$). However, the CTL run did underestimate GPP in tropical regions and overestimate it in mid- and high-latitude regions (Figure 5a, Table 2). When the dynamic rooting scheme was incorporated, the NEW run substantially eliminated underestimation in tropical regions, especially for South America, central Africa, and Southeast Asia (Figure 5b, Table 2), which are denoted as R2, R3, and R5 respectively. In addition, the overestimation of high latitudes was overcome to some extent in the areas denoted as R1 in North America and R2 in Northern Europe and Russia (Figure 5d). With further analyses, it was found that the dynamic rooting scheme can reduce soil water stress (i.e., β_t; see Section 2.1.2) in tropical areas (not shown), thus alleviating water deficiency. This development would promote photosynthesis, ultimately increasing GPP in these regions. On the other hand, increased water stress at high latitudes caused GPP to decrease. Globally, the total GPP for the CTL run was 114 Pg C year^{-1}, and for the MTE product, it was 133 Pg C year^{-1}. For the NEW run, the annual GPP increased to 118 Pg C year^{-1}, showing that the dynamic rooting scheme improved underestimation in most tropical regions, bringing it closer to MTE. The mean GPP values of the NEW run for the five typical regions were 2.94 Pg C year^{-1}, 15.33 Pg C year^{-1}, 9.46 Pg C year^{-1}, 3.95 Pg C year^{-1}, and 4.90 Pg C year^{-1}, with the highest GPP in R2 (located in South America), followed by R3 in South Africa; South Africa is fairly humid (with annual precipitation over 800 mm) and mainly covered by broadleaf trees, grass, and crops. These values were closer to MTE_GPP, with 2.99 Pg C yearyear^{-1}, 15.33 Pg C year^{-1}, 10.67 Pg C year^{-1}, 4.01 Pg C year^{-1}, and 4.87 Pg C year^{-1}. Table 2 shows the statistical characteristics of the two simulations. Clearly, the NEW run did not show apparent improvement in the correlation coefficient, but significantly reduced the MBEs and RMSEs of GPP for the five typical regions. This collection of results proved that the GPP simulation could be improved by the NEW run, reflecting the success of the dynamic rooting scheme in the coupled model.

Table 2. Statistical characteristics of annual GPP for the five grouped regions compared to MTE data. (Values with asterisks represent *R* values with significance at the 95% confidence level ($p < 0.05$), and the units for MBE and RMSE are g C m^{-2} year^{-1}.)

	R1		R2		R3		R4		R5	
	CTL	NEW	CTL	NEW	CTL	NEW	CTL	NEW	CTL	NEW
R	0.98 *	0.98 *	0.70	0.82	0.60	0.50	0.98 *	0.98 *	0.96 *	0.97 *
MBE	1.09	0.05	−7.28	−5.04	−2.41	−1.21	2.77	0.06	−1.17	0.03
RMSE	2.29	0.25	8.01	6.06	2.44	1.25	2.79	0.46	1.22	0.30

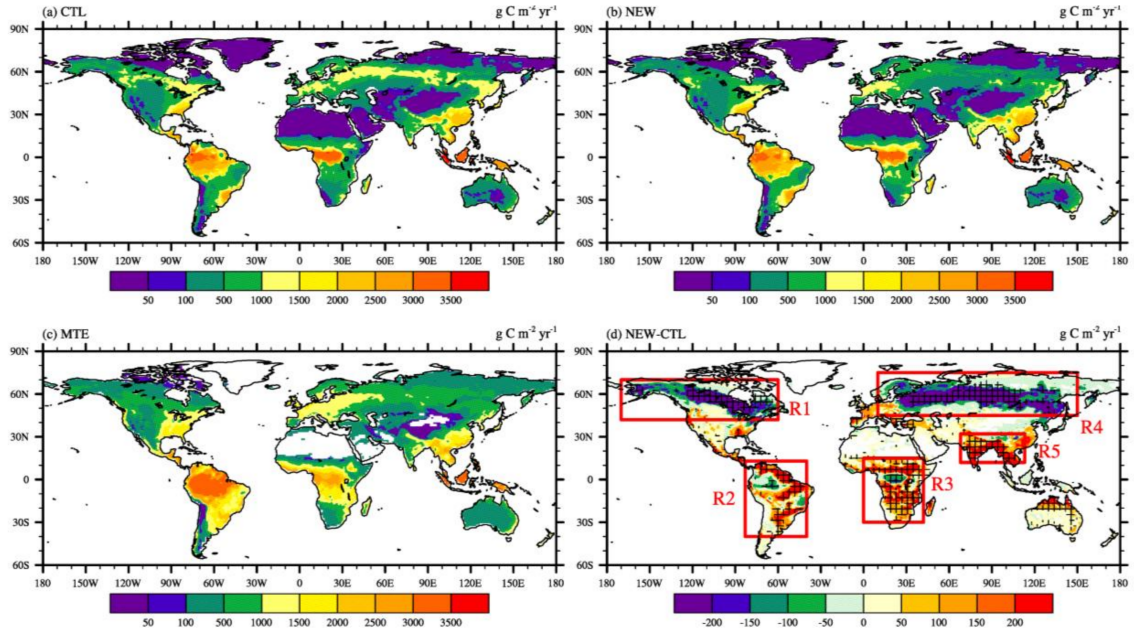

Figure 5. Annual gross primary production (GPP, g C m^{-2} $year^{-1}$) over 1982–2005 for: (**a**) the CTL run; (**b**) the NEW run; (**c**) MTE; (**d**) the difference between NEW and CTL. (Grid shaded regions are significant at the 95% confidence level according to Student's *t*-test, and red frames outline grouped regions with significant differences, denoted as R1, R2, R3, R4, and R5.).

3.2. Effects on Atmospheric Variables

Air temperature and precipitation are two basic physical quantities for characterizing climate state, and are also two important indicators for evaluating the performance of atmospheric or climate models [39]. Figure 6 shows the distribution of 24-year mean 2-m air temperature (TA). It is apparent that both runs could reasonably reproduce the global distribution of TA (Figure 6a,b), which is characterized by TA being highest in low-latitude regions, gradually decreasing from the Equator to the Poles, being low in the Qinghai-Tibet Plateau and other large land areas, and consistent with NCEP data (Figure 6c). When considering the root dynamic distribution, the NEW run showed a greater or lesser decrease in TA in most parts of the world, especially for low-latitude regions (with 95% confidence level) such as South Asia, the Amazon, and South Africa. TA decreased up to 2 °C in these regions, mainly due to the apparent increase in evapotranspiration (see Section 3.1), which increased the latent heat flux. As a result, overall, the land released more heat to the atmosphere, resulting in cooling of the land surface and lower SH (see Section 3.1). Because the lower atmosphere is heated mainly by long-wave radiation emitted from the land surface, ultimately, the decrease in surface temperature in low latitudes reduced the TA in the corresponding area, resulting in a cooling effect.

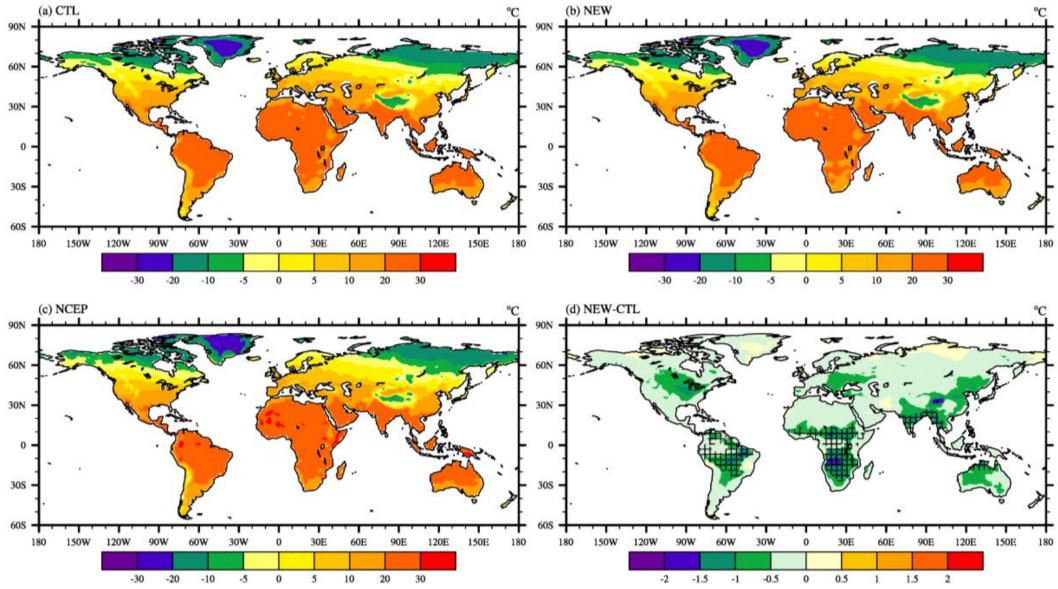

Figure 6. Twenty-four-year (1982–2005) mean 2-m air temperature (TA, °C) from (**a**) the CTL run; (**b**) the NEW run; (**c**) NCEP data; (**d**) the difference between NEW and CTL. (Grid shaded regions are significant at the 95% confidence level according to Student's *t*-test.).

Figure 7 shows the spatial distribution of global 24-year mean precipitation. Both runs showed a similar pattern for global precipitation, consistent with GPCC data (Figure 7a–c), with the heaviest precipitation distributed mainly in tropical regions, the Americas, and the east coast of Asia, which is affected by the summer monsoon and typhoons. However, North Africa, arid deserts, and the polar regions had relatively less precipitation. The differences in total precipitation between the two experiments were mainly concentrated in tropical regions. In the northeastern part of the Amazon and the west coast of Africa, total precipitation increased by 200 mm year^{-1}, and in South America, central Africa, and Indonesia, total precipitation increased by 50 to 100 mm year^{-1} (Figure 7c). Compared with the GPCC, the new scheme partly overcame the underestimation of total precipitation over the northeastern Amazon, Indonesia, and the overestimation over south Asia. Figure 7d,e show the difference in large-scale and convective precipitation between NEW and CTL respectively. It is obvious that both large-scale and convective precipitation have consistent changes with regard to the total precipitation. In the northeastern Amazon, convective precipitation contributes more to the increase in total precipitation, which implies that in this area local climate changes result in the more frequent occurrence of convective weather, and in the west coast of central Africa large precipitation events contribute more to total precipitation.

Generally, precipitation in a region is affected not only by local land-surface feedback, but also by large-scale moisture advection. However, the advection process itself may still be affected by the land–atmosphere interaction. Incorporation of the dynamic rooting scheme changes root water absorption, and therefore the temporal and spatial variation of soil moisture, ultimately affecting the calculation of terrestrial water fluxes. Advection processes then redistribute the water and energy toward the surface, and finally influence the upper atmospheric circulation. For precipitation, rising motion and vapor are two key factors. Vapor is mainly concentrated in the lower atmosphere, which is the source of precipitation. Weather systems in the lower atmosphere also play an important part in creating precipitation. The most suitable pressure for analyses is 850 hPa which can also avoid the impact of terrain. Figure 8 shows, for comparison, an 850 hPa wind field and the water-vapor flux that had a direct influence on the precipitation calculations of the two runs. The water-vapor flux (Q) was calculated as:

$$\vec{Q} = \frac{1}{g}\int_{100}^{P_s} \vec{V} \cdot q dp = \frac{1}{g}\int_{100}^{P_s} (\vec{u}, \vec{v}) \cdot q dp \quad (9)$$

where u and v represent the zonal and meridional wind speeds (m s^{-1}) respectively, q is the specific humidity (g kg^{-1}), and P_s is the surface pressure (hPa).

It was obvious that the NEW run changed the global low-level wind field (Figure 8a) by 1–2 m s^{-1}, mainly in tropical regions. In addition, more water vapor is present in the tropical atmosphere, and therefore water-vapor transport comes mainly from low-latitude areas. For example, warm air carrying water vapor from the sea results in more precipitation in Indonesia, central Africa, and the northern coast of South America; contrarily, in the southern region of India and southern China, there is less precipitation, mainly because of cold and dry air coming from northern Asia (Figure 7b,d). In the northeastern part of the Amazon, the west coast of Africa, and Indonesia, due to moisture convergence, large-scale continuous precipitation was increased by 100–200 mm $year^{-1}$. In South Asia, anticyclonic circulation led to a large water-vapor divergence, thereby reducing large-scale continuous rainfall by up to 100 mm $year^{-1}$ (Figure 7e). On the other hand, in the northeastern Amazon, the west coast of Africa, and Indonesia, due to increased evapotranspiration (Figure 4b), convective rain also increased (Figure 7f). Overall, local land-surface feedback and large-scale moisture advection resulted in an increase in total regional atmospheric precipitation, causing the humidifying effect.

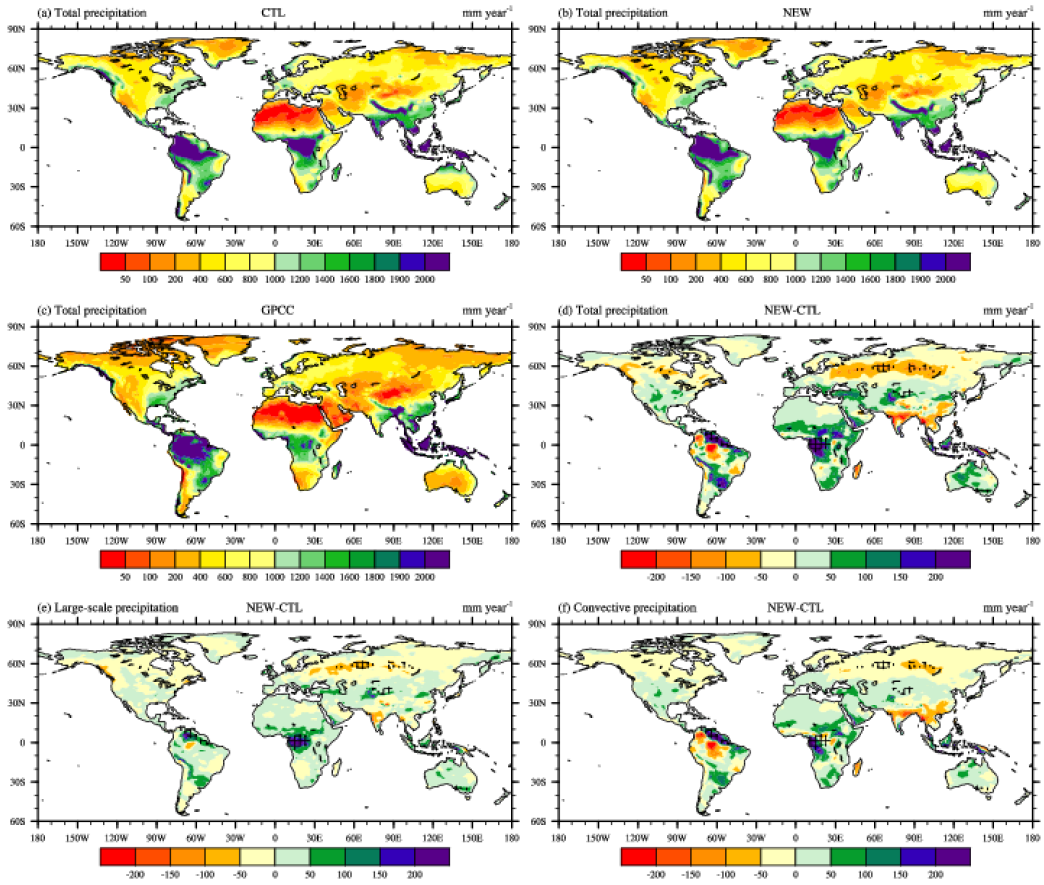

Figure 7. Twenty-four-year (1982–2005) mean precipitation (PR, mm $year^{-1}$) for (**a**) total precipitation of the CTL run; (**b**) total precipitation of the NEW run; (**c**) total precipitation from GPCC (**d**) difference in total precipitation between NEW and CTL; (**e**) difference in large-scale precipitation between NEW and CTL; (**f**) difference in convective precipitation between NEW and CTL. (Grid shaded regions are significant at the 95% confidence level according to Student's *t*-test.).

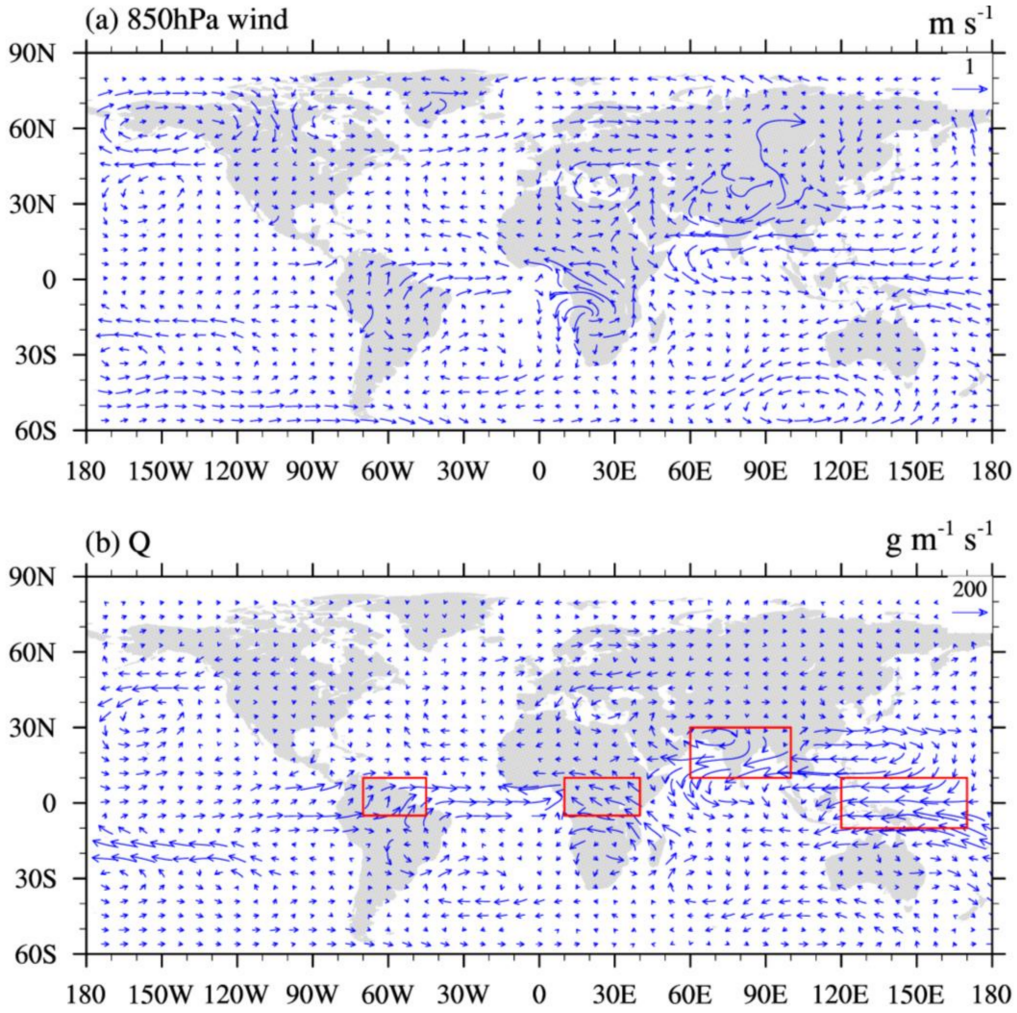

Figure 8. Twenty-four-year (1982–2005) mean difference of: (**a**) 850 hPa wind field (m s^{-1}); (**b**) water-vapor flux (g m^{-1} s^{-1}).

4. Conclusions

In this study, a dynamic rooting scheme describing root growth as a compromise between water and nitrogen availability in the subsurface was incorporated into CESM1.2.0, and its effects on global climate modelling were evaluated. Comparative analysis revealed that when the dynamic root distribution was considered, soil water stress decreased in most tropical regions, but increased in high-latitude regions. The proposed model can not only reduce GPP and ET overestimation in high-latitude areas, but also can reduce GPP and ET underestimation in tropical and subtropical regions. Due to the apparent increase in evapotranspiration in tropical regions, the 2-m air temperature decreased, resulting in a cooling effect of up to 2 °C. As for precipitation, which is affected by local land-surface feedback and large-scale moisture advection, total precipitation in the northeastern Amazon and the west coast of Africa increased by 200 mm $year^{-1}$, whereas precipitation in South America, central Africa, and Indonesia increased by 50–100 mm $year^{-1}$. Overall, the model incorporating the dynamic rooting scheme may reveal cooling and humidifying effects, especially for tropical regions. In addition to the dynamic rooting scheme, many other root-related mechanisms, including deep root systems extending up to 18 m [40], hydraulic redistribution [41], and preferential root water uptake [6], also contribute to water uptake, and consequently interact with climate; hence, they should be further examined in modeling studies. This paper presents preliminary comparisons of

the effects of dynamic root distribution on eco-hydrology and global climate. A more in-depth analysis of the effects of other root-related properties at the global scale is needed in the future.

Acknowledgments: This research was supported by the National Key Research and Development Program of China (2016YFA0600203), the Key Research Program of Frontier Sciences, CAS (QYZDY-SSW-DQC012), and the National Natural Science Foundation of China (Grant No. 41575096). The authors would like to thank the editor and the reviewers for their constructive comments and suggestions on the paper.

Author Contributions: Y.W. and B.J. designed the study; Y.W. analyzed the data with help of B.J. Y.W. wrote the paper with contributions from Z.X. and B.J.

Conflicts of Interest: The authors declare no conflicts of interest.

References

1. Chase, T.N.; Pielke, R.A.; Kittel, T.G.F.; Nemani, R.; Running, S.W. The sensitivity of a general circulation model to global changes in leaf area index. *J. Geophys. Res.* **1996**, *101*, 7393–7408. [CrossRef]
2. Betts, R.A.; Cox, P.M.; Lee, S.E.; Woodward, F.I. Contrasting physiological and structural vegetation feedbacks in climate change simulations. *Nature* **1997**, *387*, 796–800. [CrossRef]
3. Fu, C.B.; Dong, W.J.; Wen, G.; Ye, D.Z.; Ji, J.J.; Lu, J.H.; Yan, X.D. Regional response and adaption to global change. *Acta Meteorol. Sin.* **2003**, *61*, 245–249. [CrossRef]
4. Yuan, F. Hydrological Process Modeling Considering the Effects of Vegetation. Ph.D. Thesis, Hohai University, Nanjing, China, 2006.
5. Wang, Y.P.; Law, R.M.; Pak, B. A global model of carbon, nitrogen and phosphorus cycles for the terrestrial biosphere. *Biogeosciences* **2010**, *7*, 2261–2282. [CrossRef]
6. Lai, C.; Katul, G. The dynamic role root-water uptake in coupling potential to actual transpiration. *Adv. Water Resour.* **2000**, *23*, 427–439. [CrossRef]
7. Zeng, X.B.; Dai, Y.J.; Dickinson, R.E.; Shaikh, M. The role of root distribution for climate simulation over land. *Geophys. Res. Lett.* **1998**, *25*, 4533–4536. [CrossRef]
8. Feddes, R.A.; Hoff, H.; Bruen, M.; Dawson, T.; Rosnay, P.D.; Dirmeyer, P.; Jackson, R.B.; Kabat, P.; Kleidon, A.; Lilly, A. Modeling root water uptake in hydrological and climate models. *Bull. Am. Meteor. Soc.* **2001**, *82*, 2797–2810. [CrossRef]
9. El Maayar, M.; Sonnentag, O. Crop model validation and sensitivity to climate change scenarios. *Clim. Res.* **2009**, *39*, 47–59. [CrossRef]
10. Bonan, G.B. *A Land Surface Model (LSM Version 1.0) for Ecological, Hydrological, and Atmospheric Studies: Technical Description and User's Guide. Tech. Note NCAR/TN-417-STR*; National Center for Atmospheric Research: Boulder, CO, USA, 1996. Available online: https://daac.ornl.gov/data/model_archive/LSM/comp/NCAR_LSM_Users_Guide.pdf (accessed on 1 March 2018).
11. Zeng, X.B.; Shaikh, M.; Dai, Y.J.; Dickinson, R.E.; Myneni, R. Coupling of the common land model to the NCAR community climate model. *J. Clim.* **2002**, *15*, 1832–1854. [CrossRef]
12. Ivanov, V.Y.; Bras, R.L.; Vivoni, E.R. Vegetation hydrology dynamics in complex terrain of semiarid areas: 1.A mechanistic approach to modeling dynamic feedbacks. *Water Resour. Res.* **2008**, *44*, W03429. [CrossRef]
13. Nepstad, D.C.; Carvalho, C.R.D.; Davidson, E.A.; Jipp, P.H.; Lefebvre, P.A.; Negreiros, G.H.; da Silva, E.D.; Stone, T.A.; Trumbore, S.E.; Vieira, S. The role of deep roots in the hydrological and carbon cycles of Amazonian forests and pastures. *Nature* **1994**, *372*, 666–669. [CrossRef]
14. Jackson, R.B.; Mooney, H.A.; Schulze, E.D. A global budget for fine root biomass, surface area, and nutrient contents. *Proc. Natl. Acad. Sci. USA* **1997**, *94*, 7362–7366. [CrossRef] [PubMed]
15. Dickinson, R.E.; Shaikh, M.; Bryant, R.; Graumlich, L. Interactive canopies for a climate model. *J. Clim.* **1998**, *11*, 2823–2836. [CrossRef]
16. Barlage, M.; Zeng, X.B. Impact of observed vegetation root distribution on seasonal global simulations of land surface processes. *J. Geophys. Res.* **2004**, *109*, D09101. [CrossRef]
17. Zheng, Z.; Wang, G.L. Modeling the dynamic root water uptake and its hydrological impact at the Reserva Jaru site in Amazonia. *J. Geophys. Res.* **2007**, *112*, G04012. [CrossRef]
18. Jing, C.Q.; Li, L.; Chen, X.; Luo, G.P. Comparison of root water uptake functions to simulate surface energy fluxes within a deep-rooted desert shrub ecosystem. *Hydrol. Process.* **2014**, *28*, 5436–5449. [CrossRef]

19. Warren, J.M.; Hanson, P.J.; Iversen, C.M.; Kumar, J.; Walker, A.P.; Wullschleger, S.D. Root structural and functional dynamics in terrestrial biosphere models-evaluation and recommendations. *New Phytol.* **2015**, *205*, 59–78. [CrossRef] [PubMed]
20. Hutchings, M.J.; Kroon, H.D. Foraging in plants: The role of morphological plasticity in resource acquisition. *Adv. Ecol. Res.* **1994**, *25*, 159–238. [CrossRef]
21. Coelho, F.E.; Or, D. A model for soil water and matric potential distribution under drip irrigation with water extraction by roots. *Pesqui. Agropecu. Bras.* **1999**, *34*, 225–234. [CrossRef]
22. Collins, D.B.G.; Bras, R.L. Plant rooting strategies in water-limited ecosystems. *Water Resour. Res.* **2007**, *43*, W06407. [CrossRef]
23. Sivandran, G.; Bras, R.L. Dynamic root distributions in ecohydrological modeling: A case study at Walnut Gulch Experimental Watershed. *Water Resour. Res.* **2013**, *49*, 3292–3305. [CrossRef]
24. McMurtrie, R.E.; Iversen, C.M.; Dewar, R.C.; Medlyn, B.E.; Näsholm, T.; Pepper, D.A.; Norby, R.J. Plant root distributions and nitrogen uptake predicted by a hypothesis of optimal root foraging. *Ecol. Evol.* **2012**, *2*, 1235–1250. [CrossRef] [PubMed]
25. Schenk, H.J.; Jackson, R.B. The global biogeography of roots. *Ecol. Monogr.* **2002**, *72*, 311–328. [CrossRef]
26. Schenk, H.J. The shallowest possible water extraction profile: A null model for global root distributions. *Vadose Zone J.* **2008**, *7*, 1119–1124. [CrossRef]
27. Smithwick, E.A.H.; Lucash, M.S.; McCormack, M.L.; Sivandran, G. Improving the representation of roots in terrestrial models. *Ecol. Model.* **2014**, *291*, 193–204. [CrossRef]
28. Wang, Y.Y.; Xie, Z.H.; Jia, B.H. Incorporation of a Dynamic Root Distribution into CLM4.5: Evaluation of Carbon and Water fluxes over the Amazon. *Adv. Atmos. Sci.* **2016**, *33*, 1047–1060. [CrossRef]
29. Hurrell, J.W.; Holland, M.M.; Gent, P.R.; Ghan, S.; Kay, J.E.; Kushner, P.J.; Lamarque, J.F.; Large, W.G.; Lawrence, D.; Lindsay, K. The Community Earth System Model: A framework for collaborative research. *Bull. Am. Meteor. Soc.* **2013**, *94*, 1339–1360. [CrossRef]
30. Neale, R.B.; Chen, C.C.; Gettelman, A.; Lauritzen, P.H.; Park, S.; Williamson, D.L.; Conley, A.J.; Garcia, R.; Kinnison, D.; Lamarque, J.F. Description of the NCAR Community Atmosphere Model (CAM 4.0). NCAR Tech. Note NCAR/TN-4851STR. 2010. Available online: http://www.cesm.ucar.edu/models/cesm1.0/cam/docs/description/cam4_desc.pdf (accessed on 1 March 2018).
31. Neale, R.B.; Richter, J.; Park, S.; Lauritzen, P.H.; Vavrus, S.J.; Rasch, P.J.; Zhang, M.H. The mean climate of the Community Atmosphere Model (CAM4) in forced SST and fully coupled experiments. *J. Clim.* **2013**, *26*, 5150–5168. [CrossRef]
32. Lawrence, D.M.; Oleson, K.W.; Flanner, M.G.; Thornton, P.E.; Swenson, S.C.; Lawrence, P.J.; Zeng, X.; Yang, Z.L.; Levis, S.; Sakaguchi, K. Parameterization Improvements and Functional and Structural Advances in Version 4 of the Community Land Model. *J. Adv. Model. Earth Syst.* **2011**, *3*, M03001. [CrossRef]
33. Oleson, K.W.; Lawrence, D.M.; Bonan, G.B.; Drewniak, B.; Huang, M.; Koven, C.D.; Levis, S.; Li, F.; Riley, J.; Subin, M. *Technical Description of Version 4.5 of the Community Land Model (CLM). NCAR Tech. Note NCAR/TN-503+STR*; National Center for Atmospheric Research: Boulder, CO, USA, 2013; p. 420.
34. Zeng, X.B. Global vegetation root distribution for land modeling. *J. Hydrometeorol.* **2001**, *2*, 525–530. [CrossRef]
35. Shangguan, W.; Dai, Y.J.; Duan, Q.Y.; Liu, B.Y.; Yuan, H. A global soil data set for earth system modeling. *J. Adv. Model. Earth Syst.* **2014**, *6*, 249–263. [CrossRef]
36. Rayner, N.A.; Parker, D.E.; Horton, E.B.; Folland, C.K.; Alexander, L.V.; Rowell, D.P.; Kent, E.C.; Kaplan, A. Global analyses of sea surface temperature, sea ice, and night arine air temperature since the late nineteenth century. *Geophys. Res.* **2003**, *108*, 4407. [CrossRef]
37. Jung, M.; Reichstein, M.; Bondeau, A. Towards global empirical upscaling of FLUXNET eddy covariance observations: Validation of a model tree ensemble approach using a biosphere model. *Biogeosciences* **2009**, *6*, 2001–2013. [CrossRef]
38. Jung, M.; Reichstein, M.; Margolis, H.A.; Cescatti, A.; Richardson, A.D.; Arain, M.A.; Arneth, A.; Bernhofer, C.; Bonal, D.; Chen, J. Global patterns of land-atmosphere fluxes of carbon dioxide, latent heat, and sensible heat derived from eddy covariance, satellite, and meteorological observations. *J. Geophys. Res.* **2011**, *116*, G00J07. [CrossRef]

39. Shi, X.L.; Zhang, F.; Zhou, W.Y.; Zhang, Y. Impacts of CG-LTDR Land Cover Dataset Updates on the Ground Temperature Simulation with BCC_AVIM 1.0. *J. Geo-Inf. Sci.* **2015**, *11*, 1294–1303. [CrossRef]
40. Canadell, J.; Jackson, R.B.; Ehleringer, J.R.; Mooney, H.A.; Sala, O.E.; Schulze, E.D. Maximum rooting depth of vegetation types at the global scale. *Oecologia* **1996**, *108*, 583–595. [CrossRef] [PubMed]
41. Ryel, R.J.; Caldwell, M.M.; Yoder, C.K.; Or, D.; Leffler, A. Hydraulic redistribution in a stand of Artemisia tridentate: Evaluation of benefits to transpiration assessed with a simulation model. *Oecologia* **2002**, *130*, 173–184. [CrossRef] [PubMed]